ULTRASONIC DETECTION AND IDENTIFICATION OF FABRICATION DEFECTS IN COMPOSITES

Edward R. Long, Jr.
NASA Langley Research Center

Susan M. Kullerd
Lockheed Engineering and Sciences Company

Patrick H. Johnston
NASA Langley Research Center

and

Eric I. Madaras
NASA Langley Research Center

SUMMARY

Methods for deliberate fabrication of porosity into carbon/epoxy composite panels and the influence of three-dimensional stitching on the detection of porosity have been investigated. Two methods of introducing porosity were studied. Porosity was simulated by inclusion of glass microspheres and a more realistic form of porosity was introduced by using low pressure during consolidation. The panels were ultrasonically scanned and the frequency slope of the ultrasonic attenuation coefficient was used to evaluate the two forms of porosity. The influence of stitching on detection of porosity was studied using panels which were resin transfer molded from stitched plies of knitted carbon fabric and epoxy resin.

INTRODUCTION

Porosity in carbon fiber reinforced polymeric composites (CFRPC) caused by improper processing during fabrication has been shown to degrade the materials' mechanical performances (ref. 1-2). Therefore, methods of nondestructive evaluation (NDE) for the detection and identification of porosity are important. Ultrasonic signal attenuation is a popular NDE method for imaging and identifying porosity in CFRPC and it has been the subject of a number of recent NDE studies (ref. 3-8).

Porosity is caused by air or volatile chemical species which are not adequately released from the part during fabrication because vacuum and/or pressure is insufficient at critical points during the

cure cycle. For composites fabricated from prepreg, voids typically occur at ply interfaces and they tend to aggregate, more or less, along the direction of the fibers depending on ply orientations. Therefore, the extent to which mechanical properties are affected is dependent on a combination of the degree of improper fabrication and the orientations of the reinforcing fibers.

NDE studies of porosity in CFRPC are typically conducted with specimens in which the amount of porosity is controlled either by lowering the applied pressure or vacuum during fabrication or by using solid or hollow glass microspheres between plies to represent the porosity (ref. 1-8). Both methods provide individual spherical or aggregate cylindrical sites which cause similar characteristic scattering of ultrasonic energy. For that reason, both representations of voids provide similar frequency-dependent effects on the attenuation of ultrasonic energy and can be studied using an analysis of the slope of attenuation (ref. 3 and 7), which will be described below.

While the inclusion of microspheres allows control of the volume concentration of scatterers, this method may not provide a quantitative basis for establishing standards for production NDE. Solid inclusions have very different acoustic impedances from those for actual voids and it is not clear that a standard based on the solid-solid interface scattering will provide appropriate calibration values from which naturally occurring gas-solid interface scattering can be inferred. Inclusions of hollow microspheres does not adequately address this problem because it is not possible to prevent some unknown fraction of the hollow spheres from being crushed during the cure of the composite, making the amount of simulated porosity effectively unknown without subsequent destructive testing. In addition, both solid and hollow microspheres can act as nucleation points for naturally occurring porosity and microcracking. Lastly, for composites fabricated from three-dimensional fiber architectures consisting of woven, knitted, or stitched assemblies, there is no convenient method for introducing a uniform internal distribution of microspheres.

The use of three-dimensional fiber architectures presents a more fundamental problem for identifying porosity. For stitched, woven, knitted, or similar geometrical intertwining of fiber tows, the tows tend to stay bundled and to form concave- or convex-shaped points of intersection which provide the same spherical or cylindrical scattering surfaces as caused by voids. Consequently, the scattering from a bundled tow or of a stitch will be similar to that from a void. Therefore, the architecture of the fibers may well provide false evidence for the existence of a defect. If this would be the case, then "physics-based" methods for defect identification, such as slope-of-attenuation for porosity, may have to be modified or supplemented by more sophisticated measurement techniques when three-dimensional fiber architectures are involved.

This paper discusses recent results from ongoing research at NASA Langley Research Center to study methods for controlled representations of fabrication defects and to study the effects of three-dimensional fiber architectures on defect detection. Porosity is currently under investigation, with low-pressure and microspherical void representation being comparatively studied. The architecture of the fiber reinforcement under current study is a stitched, knitted carbon fabric and its effects on the detection of porosity are reviewed.

SPECIMEN PREPARATION

Both solid glass microspheres and low-pressure cure were used to introduce voids into the composite. The method for using low pressure is depicted in figure 1. Composite panels of AS4/3501-6* were laid up $[-45,+45]_{2S}$ using prepreg from Hercules Inc., vacuum bagged according to conventional procedures, and cured in an autoclave, using the prepreg manufacturer's recommended cure protocol, to a maintained final cure temperature of 177 ^{o}C (350 ^{o}F). A range of porosities was obtained by choosing a different curing pressure for each panel, from a low of 6.9×10^4 Pa (10 psi) to the recommended pressure of 6.9×10^5 Pa (100 psi). As may be seen from the photomicrographs in figure 1, the porosity varied from individual spherical voids at high pressure to larger elliptical or cylindrical voids at low pressure. Only the 6.9×10^4 Pa (10-psi) specimen has been studied to date.

The method for using 25.4-micron (0.001-in) diameter glass microspheres is depicted in figure 2. A 15.2-cm x 15.2-cm (6.0-in x 6.0-in) composite panel was fabricated with 8 plies of AS4/3501-6 symmetrically oriented at +45 and -45 degrees. The microspheres were located at the top right between plies 1 and 2, at the middle between plies 4 and 5, and at the lower left between plies 7 and 8. During the assembly of the prepreg plies, the microspheres were deposited in a 2.5-cm x 2.5-cm (1.0-in x 1.0-in) area by holding a template containing a square hole over the lower ply for each location and distributing microspheres from a shaker. The stack was consolidated in a press mold at 6.9×10^5 Pa (100 psi) and 177 ^{o}C (350 ^{o}F).

A stitched, knitted 15.2-cm x 15.2-cm (6.0-in x 6.0-in) panel was fabricated using a resin transfer molding technique depicted in figure 3. A 16-ply AS4/3501-6 panel, was made of knitted layers of unidirectional tows in a quasi-isotropic layup. The layers were then stitched together on 6.0-mm (0.25-in) centers in both the 0- and 90-degree directions. The 3501-6 resin was obtained from Hercules Inc. and the stitched fiber preform from Hexcel Corporation.

The details for the resin transfer process are described in another presentation at this conference (ref. 9). The panel used in this study was processed to deliberately form porosity by using a combination of 2.8 x 10^5-Pa (40-psi) instead of the required 5.6 x 10^5-Pa (80-psi) pressure and a nonheated upper platen.

EXPERIMENTAL PROCEDURE

The ultrasonic data acquisition system is depicted schematically in figure 4. Measurements were made in a water-filled tank with a motorized X-Y bridge for positioning an ultrasonic transducer pointing in the Z direction over the specimen. The panels were mounted above a sheet of flat glass, with the glass and panel lying parallel to the X-Y plane. The pulser emitted short-duration spikes, driving the transducer to launch pulses of ultrasonic energy toward the specimen along the Z-axis. Reflections of the ultrasound from the specimen and the glass behind the specimen were received by the same transducer, amplified by the receiver, and recorded by a digital oscilloscope. The digitized signals were transferred to computer and stored for subsequent display and analysis.

The set of ultrasonic reflections resulting in this system is called an A-scan. An A-scan is depicted schematically in figure 4. As shown with reference to the sketch above the A-scan, the A-scan consists of reflections from the front and rear surfaces of the specimen, any defects within the specimen, and the glass. There are also lower level scattered reflections from the internal structure of the composite, particularly the fibers. The time separation between echoes in the A-scan represent the acoustical path lengths between structures along the Z-axis and are determined by the physical distance and the ultrasonic velocity in the intervening medium.

The ultrasonic A-scan represents information in the time domain. This information can be broken into components representing different frequencies of vibration using the Fourier transformation. The squared magnitude of the resulting frequency domain function is the power spectral density, or simply the power spectrum of the signal. The power spectrum of an ultrasonic signal indicates how the ultrasonic energy is distributed among different frequency components and can be employed to investigate ultrasonic propagation phenomena, such as attenuation, which are, in general, frequency-dependent functions.

The X-Y array of the time-based peak amplitudes of the reflection from any one surface for some spatial interval between sampling points is a C-scan. For this study, C-scans were made using the amplitude of the reflection from the glass. For each sampling point, the signal passes twice through the specimen, including any flaws present at that site. C-scans were made for each panel to determine, based on the total apparent signal attenuation, the X-Y regions of the specimen for which A-scans were to be recorded. Then the A-scans were made for

specific points within those regions. Finally, Fourier transforms (FT) of the reflections from the glass were made to determine the power spectrum for each of the specific points.

SLOPE OF ATTENUATION

The analysis method based on the slope of attenuation is illustrated in figure 5. A curve representing the logarithm of a power spectrum of a glass reflection without a composite specimen in the path of the ultrasonic signal is shown as a solid line. The dot-dash curve represents the log of a power spectrum of a glass reflection for a composite specimen placed in front of the glass. Note that the amplitudes are different due to the attenuation of the sound in the sample and note also that the difference between the two power spectra varies as a function of frequency. The frequency-dependent attenuation coefficient is found from the difference between the logged power spectra which is plotted as the dotted line in figure 5.

A band width for analysis is chosen to provide sufficient signal-to-noise ratio. The vertical lines indicate the band width over which the amplitude of the reference signal power spectrum, over glass alone, is within 10 dB of its peak value. This is referred to as the 10-dB band width of the signal. In this useful band width, the attenuation curve is examined and is noted to increase approximately linearly with frequency. A linear curve fit provides a good estimation for the slope of this curve. Because porosity scatters ultrasound out of the beam by a mechanism which increases with frequency, the value of the slope of the attenuation coefficient will increase in proportion to the amount of porosity present.

RESULTS AND DISCUSSION

Microsphere and Low-Pressure Cure Representations of Porosity

Figure 6a is a C-scan for normal incidence of ultrasonic energy on the 8-ply $(+45/-45)_{2s}$ composite panel containing microspheres. The two fiber directions and, with careful inspection, the square areas in the upper right, the middle, and lower left which contain microspheres are visible. The four dark spots are images of posts which supported the panel above the glass plate.

The image in figure 6a provides one reason for concern with using glass microspheres to represent porosity. The fiber directions are visible, probably due to actual porosity which formed along the fibers during the fabrication. The squares containing microspheres are only faintly visible probably due to porosity at their boundaries, but there is nothing within the boundaries which is visibly different than in the region outside the squares. That is to say, the microspheres do not provide the same defect image as does actual porosity.

It should be noted that in order to image the microspheres the panel must be scanned at an angle of incidence less than 90 degrees with respect to the surface in a direction which also bisects the two fiber directions. In figure 6b, the angle is approximately 45 degrees. The method of scanning at an angle is discussed in reference 8. But, as can be seen from figure 6a, scanning at an angle less than 90 degrees with respect to the fiber direction is not required for imaging actual porosity. Therefore, the different scanning geometry required to image the glass beads demonstrates why glass beads are not a good representation of porosity.

One reason which is often cited in favor of using microspheres is that they provide a controlled representation of porosity (ref. 3). As may be seen in figure 7a this is not the case. Figure 7a is a photomicrograph of a cross section of the panel containing microspheres at the midplane of the panel, the center square in figure 6b. There are also concentrations of neat resin and voids in the plane containing the microspheres. This complex presence of microspheres, resin, and actual pores represents more porosity than the microspheres alone and looks more like a poor quality adhesive bond line than a region of porosity.

Figure 7b is a photomicrograph of a cross section of the panel fabricated at 10 psi. The porosity is distributed more evenly through the thickness than in figure 7a. There are regions for which there is unequal fiber/resin distribution but not to the extreme as in figure 7a in which there is almost a band of neat resin. The low-pressure configuration of porosity is more like that which actually occurs in composites due to fabrication errors.

The attenuation curves from a site over the microsphere-loaded panel and the low-pressure panel are presented in figures 8a and 8b respectively, along with the power spectra from which they were derived. Results from both types of "porosity" can be analyzed using a linear curve fit to obtain the slope of attenuation. However, as noted in the preceding discussion for figure 7, use of the microspheres also introduced voids and resin richness. This complex presence of microspheres, resin, and natural pores presents a much different loss mechanism than that provided by natural porosity. Therefore, the same concentrations of microspheres and natural porosity would not yield the same values for slopes of attenuation.

Stitched Fiber Architectures

The effects of stitching may be seen in C-scans shown in figure 9 which were made using a 0.102-cm (0.040-in) sampling interval. Figure 9a is a quasi-isotropic panel which was autoclaved from prepreg and which has no defects which could be imaged. Figure 9b is the stitched quasi-isotropic, resin transfer molded panel described earlier. For both scans, four 0.063-in diameter lead shot were placed on the upper surface in a square array to determine how well the shot could be

imaged. The four lead shot can be seen as black spots in figure 9a, but four lead shot in a similar arrray, plus two additional shot within that array, cannot be distinguished in figure 9b. (For these two scans, reflections from the front surface and the interior of panel, not including the rear surface, were used instead of reflections from the glass. Therefore, the supports holding the panel above the glass reflector plate were not imaged.) The difference in visibility of the shot points out the difficulties which will be encountered if today's current ultrasonic C-scan techniques are used to interpret the quality of composite panels fabricated from three-dimensional fiber architectures.

Figure 10 is a set of photomicrographs, at 50X, through the panel thickness for each of three areas of the stitched panel. One area is a "good area" between stitches, another is a "bad area" between stitches, and the third is the area of a through-the-thickness stitch itself.

Figure 10a shows a "good area". The fiber orientations are visible as well as regions of nonuniform distribution of fiber and resin and a small amount of microcracking.

The "bad area" is shown in figure 10b. Visible are voids as well as resin richness and microcracks. Also visible at approximately one-quarter intervals through the thickness is the thread used for knitting. The difference between the "good area" and the "bad area" would appear to be the extent of porosity. If microcracking and resin richness are included in the list of fabrication defects then there are no good areas. Thus it should be clear that the issues surrounding fabrication defects are far more complicated than just porosity.

An area containing a stitch is shown in figure 10c. There are two orientations of stitching. One orientation of the stitching is parallel to the surface of the panel and can be seen at the top of the photograph as a bundle, or tow, coming towards the viewer. The second orientation is vertical through the thickness. Also visible are microcracks around the stitch and again it is evident that fabrication defects are more complicated than just porosity.

The stitching through the thickness contributes to the complexity of the ultrasonic measurement because its sound velocity is greater than the surrounding medium. The part of the wavefront propagating through the stitch travels faster than in the surrounding material, resulting in a phase-distorted wavefront at the receiving transducer. Since the transducer sums across its face with respect to phase as well as with respect to amplitude there is a phase-cancellation effect which reduces the perceived amplitude of the signal. This explains why the parts of the C-scan in figure 9b corresponding to the intersection of stitch lines, which is where the stitching passes through the thickness, is particularly dark. The stitch running parallel to the plane of the panel distorts the local fiber geometry,

potentially causing phase-cancellation effects, as well as providing a scattering cross section which is similar to that of the voids.

Figure 11 presents the attenuation coefficients, the slopes, and the void volume fractions measured for the "good area", the "bad area", and the stitching. The void volume fractions were determined using optical analysis. The slope is slightly increased in the "bad area" relative to the "good area", in concert with its larger amount of porosity. The attenuation measured over the stitch, however, exhibits a slope that is more than double that of the "bad area", despite having less porosity.

The distortions and scatterings of ultrasonic signals caused by the stitching appear to suggest that current methods of ultrasonic characterization of porosity, such as slope of attenuation, may not be useable for three-dimensional fiber architectures unless additional advanced ultrasonic scanning techniques are developed. One advanced technique currently under investigation at Langley Research Center for use with three-dimensional fiber architectures is phase-insensitive detection (ref. 10). This technique uses an array of detectors. Each detector's sensing area is so small that the phase distortion within that area caused by the fibers oriented in the direction of the wave propagation is negligible. Therefore, the phase-cancellation effect caused by through-the-thickness oriented fibers may be eliminated.

ACKNOWLEDGMENT

The authors wish to recognize the positive support and participation of Edward C. Taylor and Carolyn J. James for this research. Both have played a significant role in the work at Langley Research Center towards establishing state-of-the-art ultrasonic capabilities for NDE of materials and structural components.

SUMMARY

A study is in progress to evaluate two methods for representing porosity in composite materials and to investigate the effects of three-dimensional fiber architectures on detection of porosity. Porosity representations were accomplished by introduction of glass microspheres between layers of fibers before fabrication and by use of reduced pressure during fabrication. Ultrasonic C-scans, Fourier transforms of the reflected ultrasonic signal, and photomicrographs of the regions of interest show that microspheres are not a good choice for representation of porosity. The same forms of data also showed that the methods which are currently in use for characterization of porosity in conventional composite laminates will not be satisfactory for characterizing porosity in composites containing three-dimensional arrays of fiber.

REFERENCES

1.- Judd, N. C.; and Wright, W. W.: Voids and Their Effects on The Mechanical Properties of Composites - - An Appraisal. SAMPE Journal, Jan/Feb 1978, pp. 10-14.

2.- Lenoe, E. M.: Effects of Voids on Mechanical Properties of Graphite Fiber Composites. U.S. Air Systems Command AD727236, 1970.

3.- Handley, S. M.; Hughes, M. S.; Miller, J. G.; and Madaras, E. I.: Characterization of Porosity in Graphite/Epoxy Composite Laminates With Polar Backscatter and Frequency Dependent Attenuation. 1987 Ultrasonic Symposium, vol. 2, 1987, pp. 827-830.

4.- Hsu, D. K.: Quantitative Evaluation of CFRP Void Contents Using Ultrasonic Attenuation and Velocity. Proceedings of the Fourth Japan-U.S. Conference on Composite Materials, Washington, DC., June 27-29, 1988, pp. 1015-1024.

5.- Fuller, M. D.; and Gammell, P. M.: Ultrasonic Characterization of Porosity in Composite Materials by Time Delay Spectroscopy. Review of Progress in Quantitative Nondestructive Evaluation, vol. 6B, 1986, pp. 1157-1163.

6.- Tittmann, B. R.; Hosten, B.; and Abel-Gawad, M.: Ultrasonic Attenuation in Carbon-Carbon Composites and the Determination of Porosity. Proceedings of the IEEE 1986 Ultrasonics Symposium, vol. 2, 1986, pp. 1047-1050.

7.- Hsu, D. K.; and Nair, S. M.: Evaluation of Porosity in Graphite-Epoxy Composite by Frequency Dependence of Ultrasonic Attenuation. Review of Progress in Quantitative Nondestructive Evaluation, vol. 6B, 1986, pp. 1185-1193.

8.- Handley, S. M.; Hughes, M. S.; Miller, J. G.; and Madaras, E. I.: An Investigation of the Relationship Between Contrast and Azimuthal Angle for Imaging Porosity in Graphite/Epoxy Composites With Ultrasonic Polar Backscatter. Proceedings of the IEEE 1988 Ultrasonics Symposium, vol. 2, 1988, pp. 1031-1034.

9.- Loos, Alfred C.; and Weideman, Mark H., et al.: Infiltration/Cure Modeling of Resin Transfer Molded Composite Materials Using Advanced Fiber Architectures. NASA CP-3104, Part 2, 1991, pp. 425-442.

10.- Johnston, Patrick H.: Phase-Insensitive Detection and the Method of Moments for Ultrasonic Tissue Characterization, Ph.D. Dissertation, Washington U., St. Louis, MO, 1985.

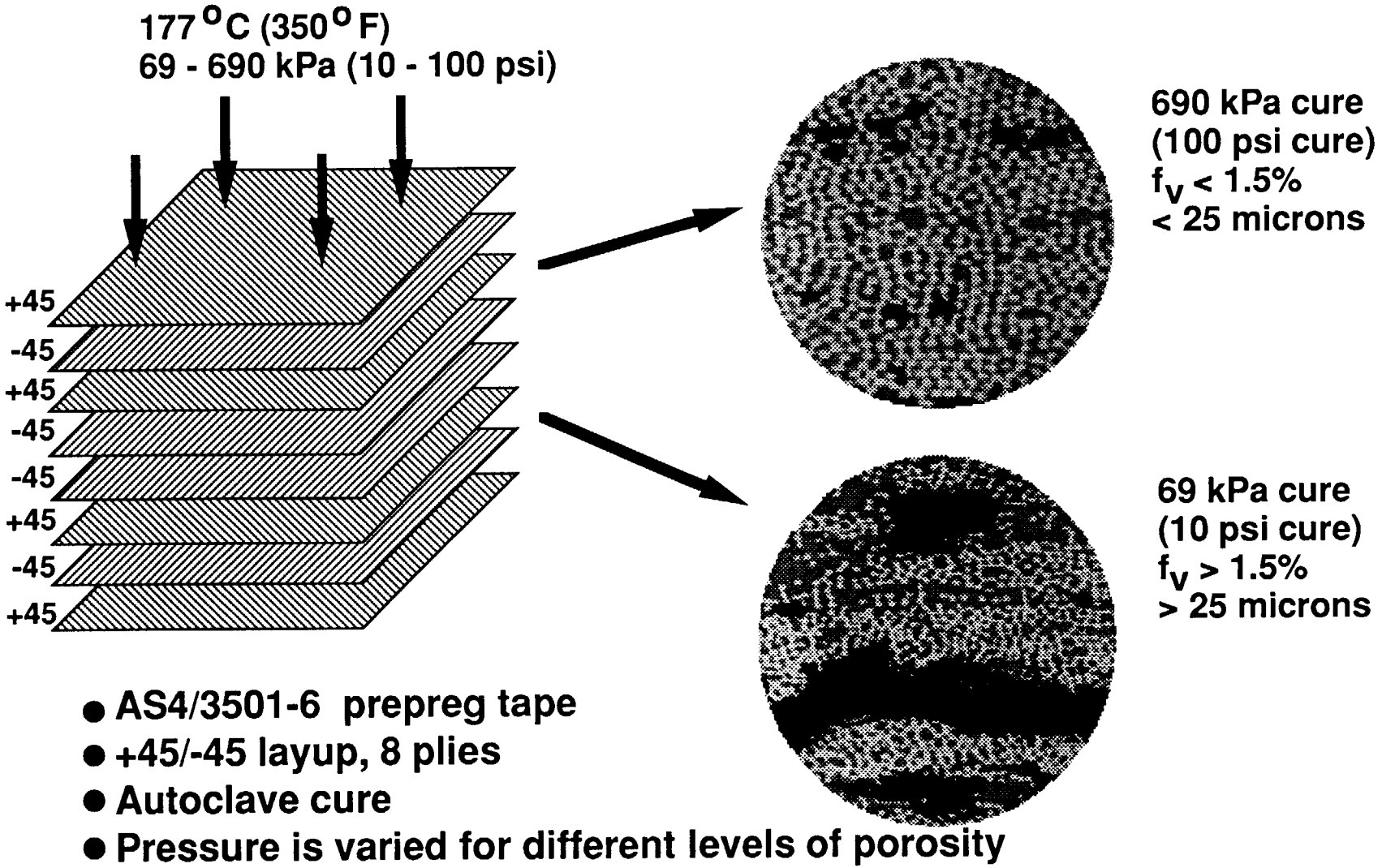

Figure 1 - Low-pressure fabrication of composite panels containing porosity.

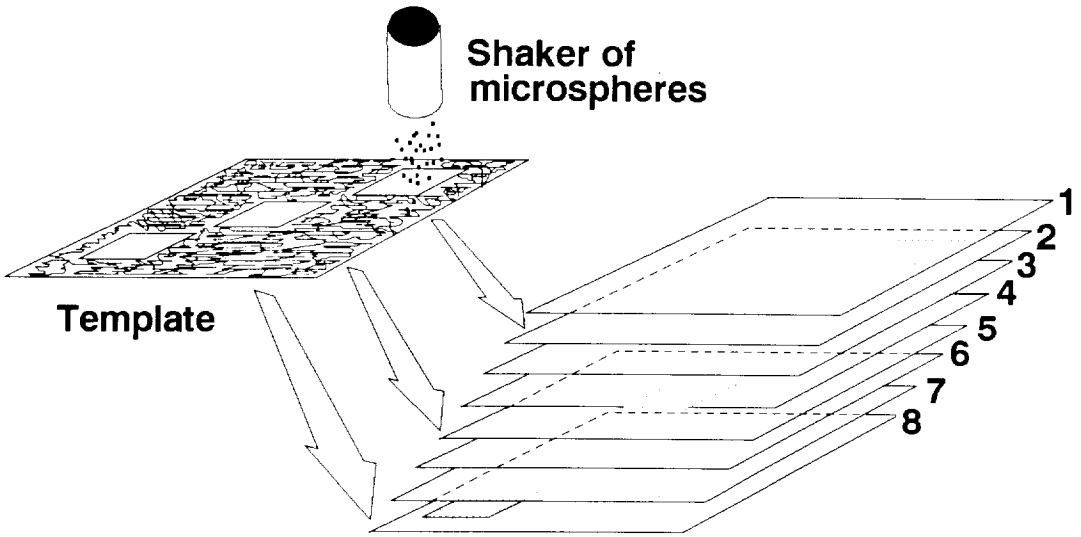

Figure 2 - Use of glass microspheres to represent localized areas containing porosity.

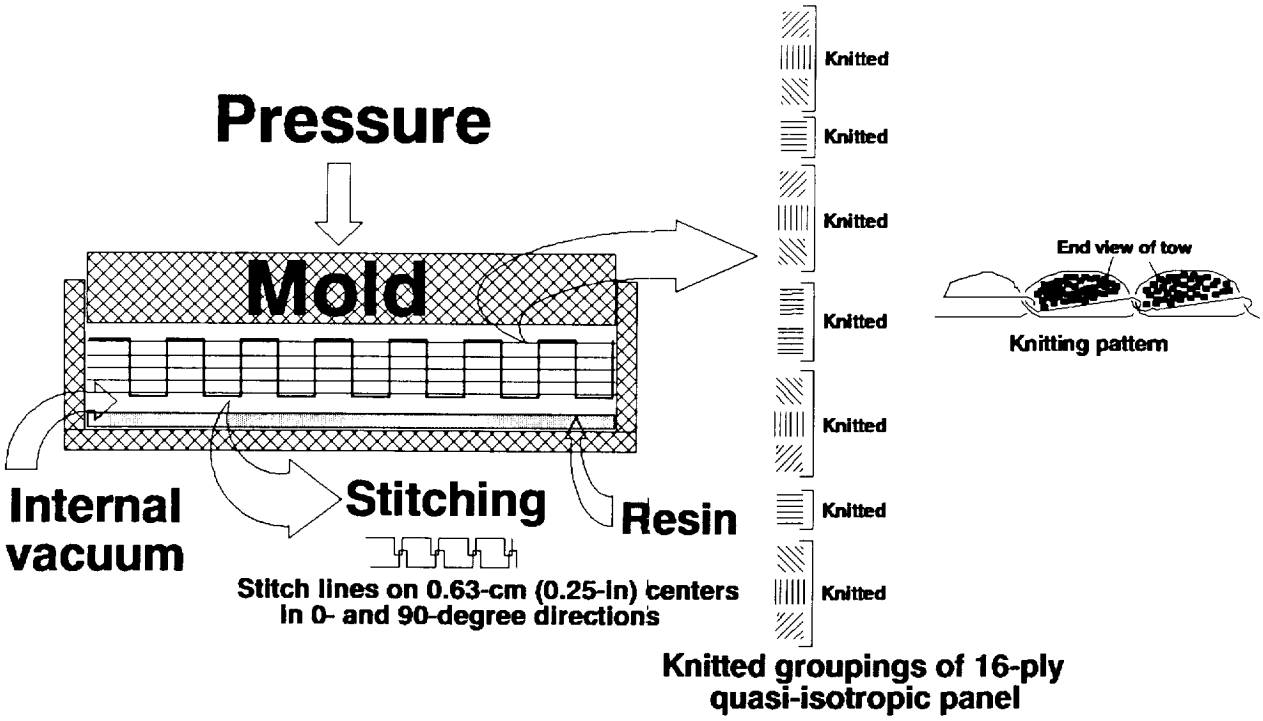

Figure 3 - Resin transfer mold fabrication of a stitched, knitted panel.

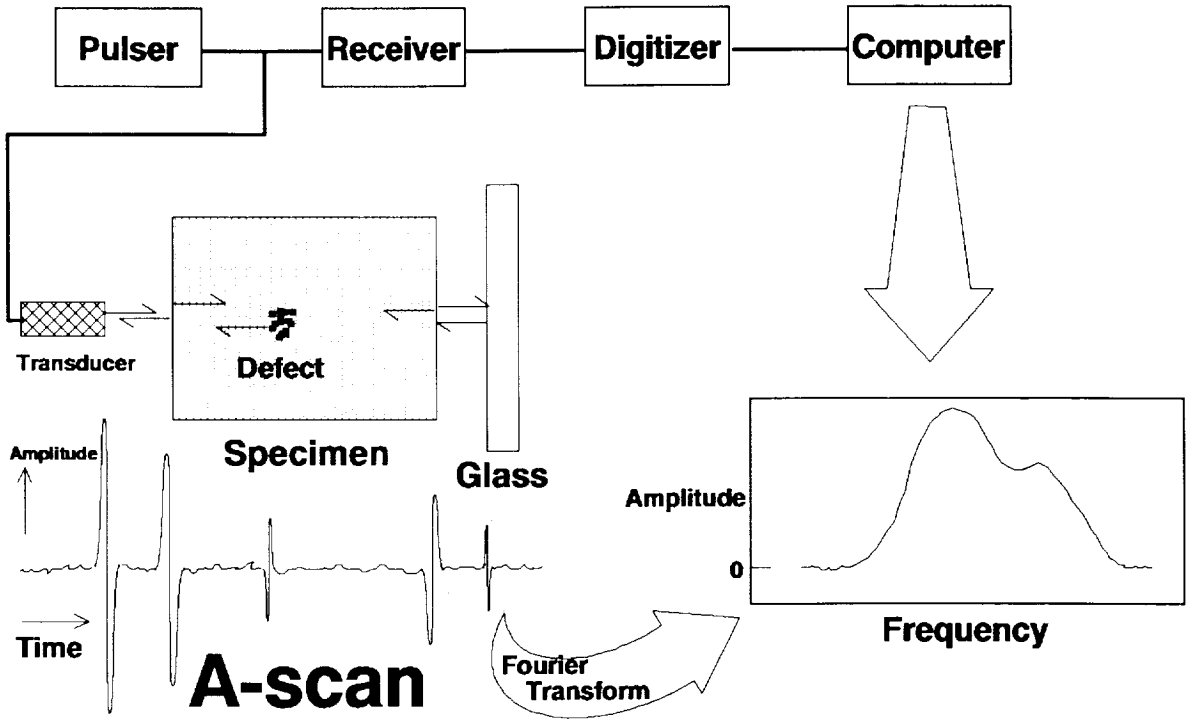

Figure 4 - Diagram of ultrasonic data acquisition system.

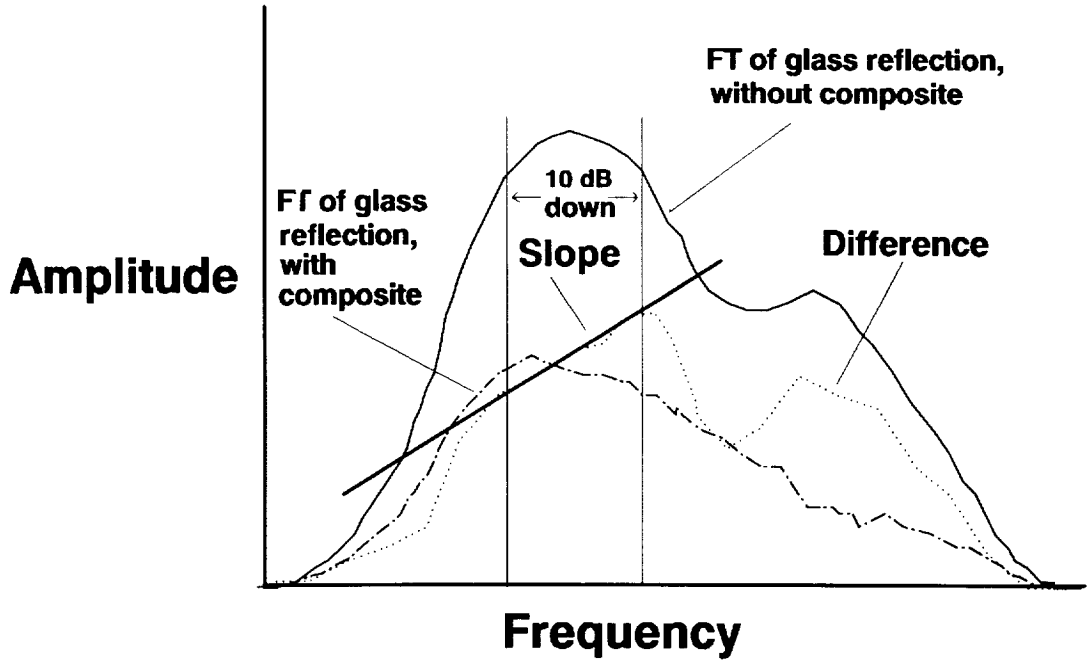

Figure 5 - Determination of slope of attenuation caused by panel defects from differences of Fourier transforms (power spectra) of reflections from the glass reflector plate with and without a composite panel in the beam path.

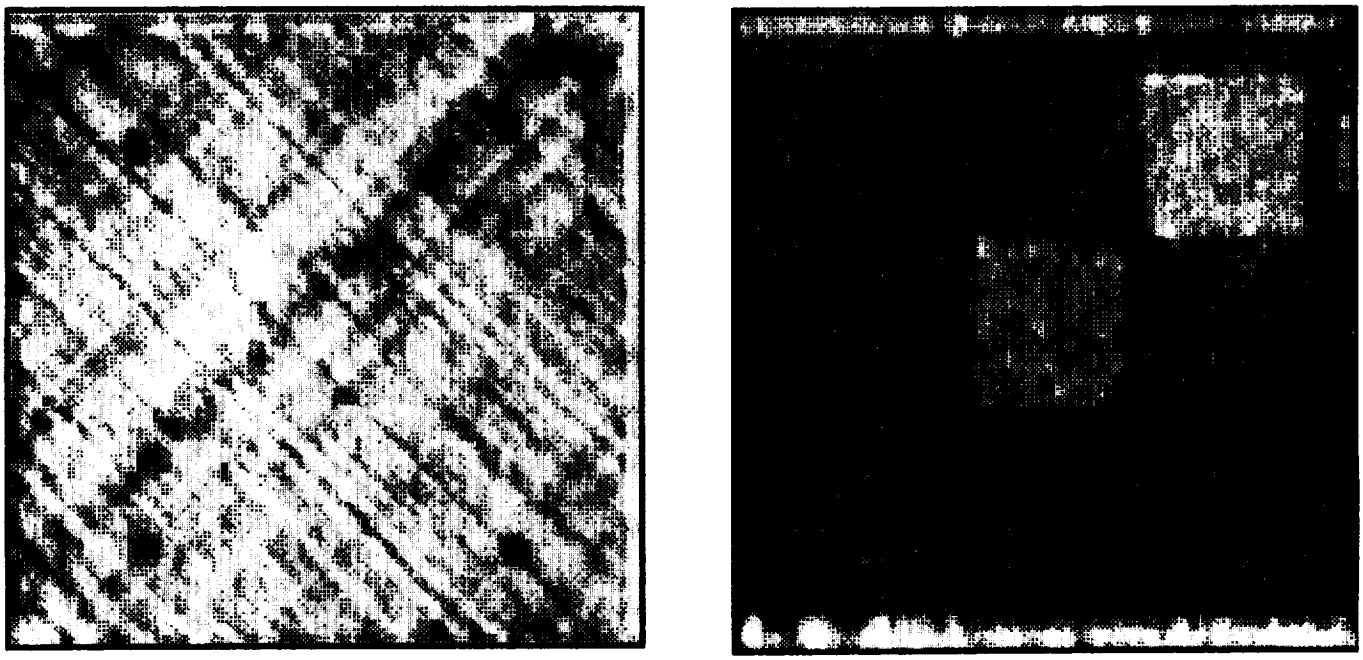

(a) Normal incidence

(b) 45-degree incident angle

Figure 6 - C-scan image of a 15.2-cm X 15.2-cm (6.0-in x 6.0-in), 8-ply, $(+45/-45)_{2s}$ panel containing 2.5-cm X 2.5-cm (1.0-in x 1.0-in) patches of glass microspheres.

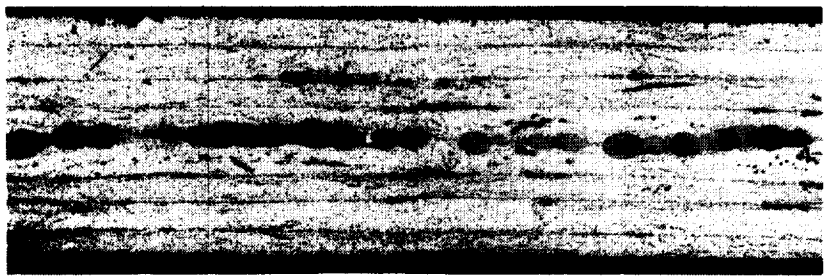

(a) Microspheres imbedded at the midplane.

(b) Porosity induced by 69 kPa (10 psi) cure. Void volume fraction: 3.5% by resin digestion (ASTM D-3171) and 4.7% by optical analysis.

Figure 7 - Photomicrographs of sections through an 8-ply, $(+45/-45)_{2s}$ graphite/epoxy composite.

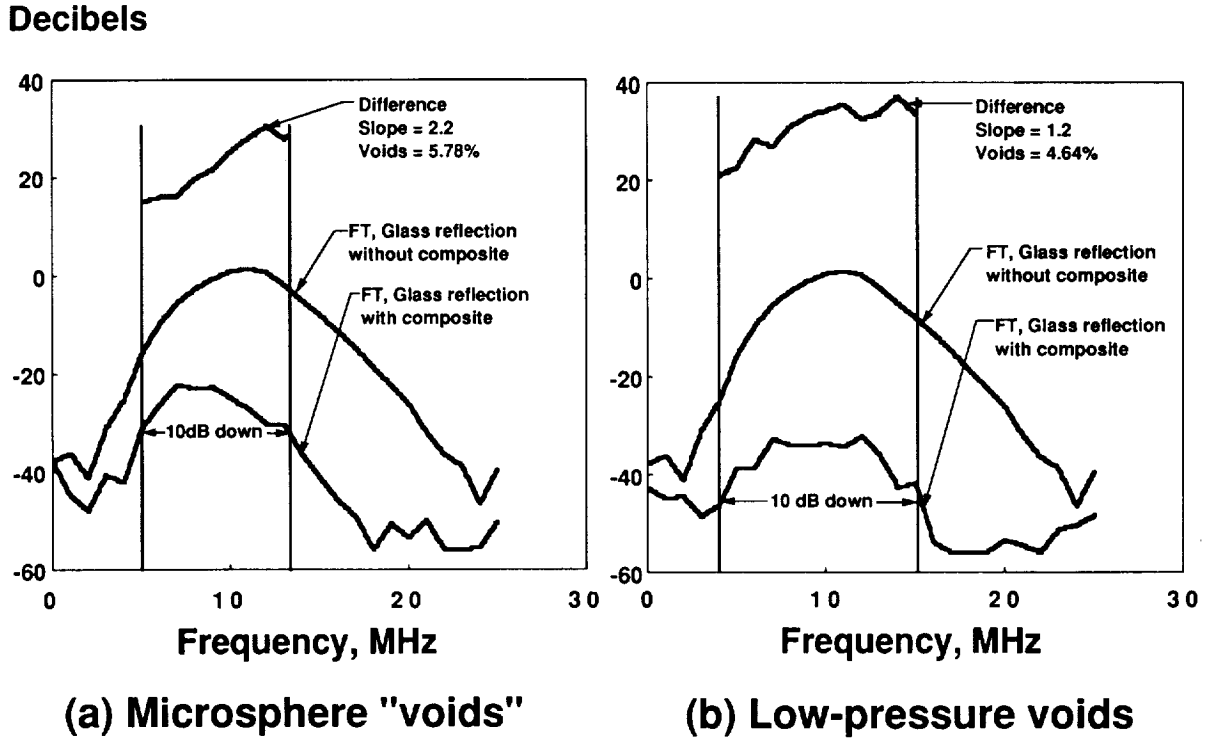

Figure 8 - Differences of Fourier transforms for glass microsphere (a) and for low-pressure (b) representations of porosity. Void content determined from optical analysis.

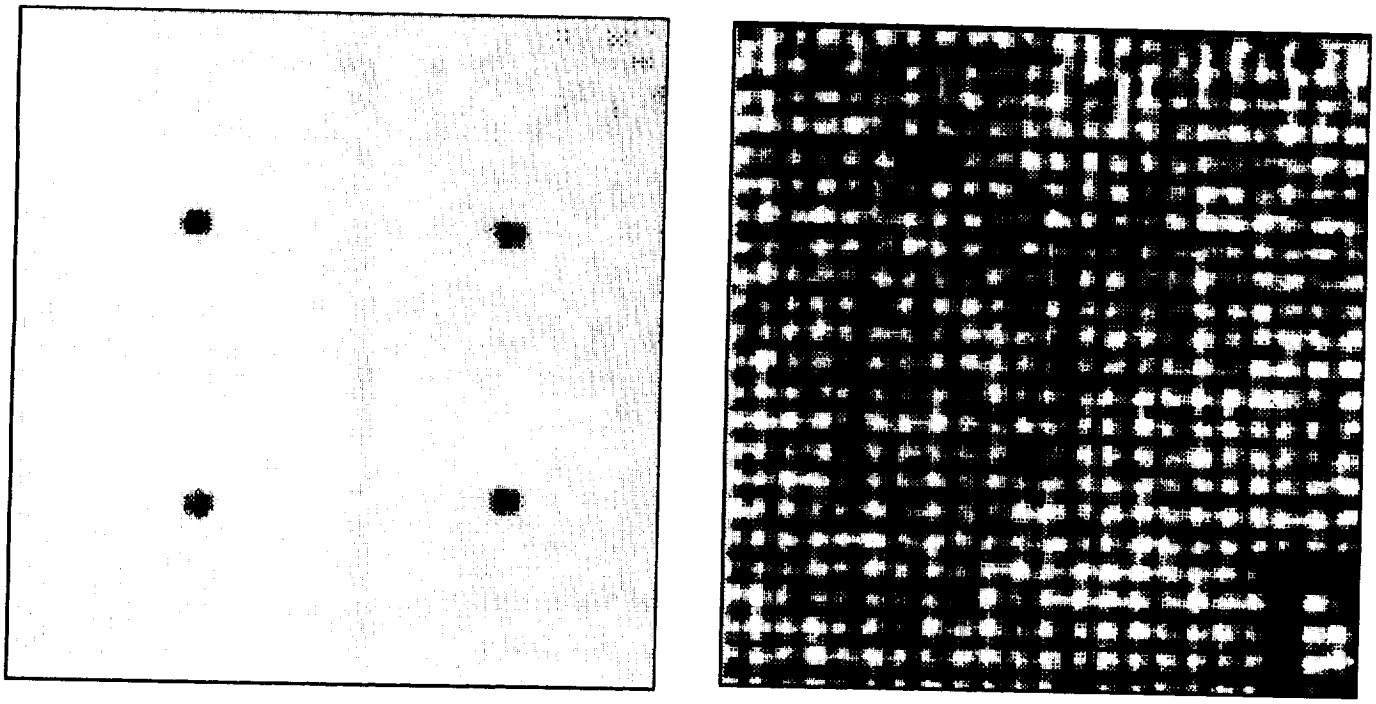

(a) Non-stitched

(b) Stitched

Figure 9 - C-scans of nonstitched and stitched panels, both having lead shot on their upper surface, using reflections from the panel's front surface and volume.

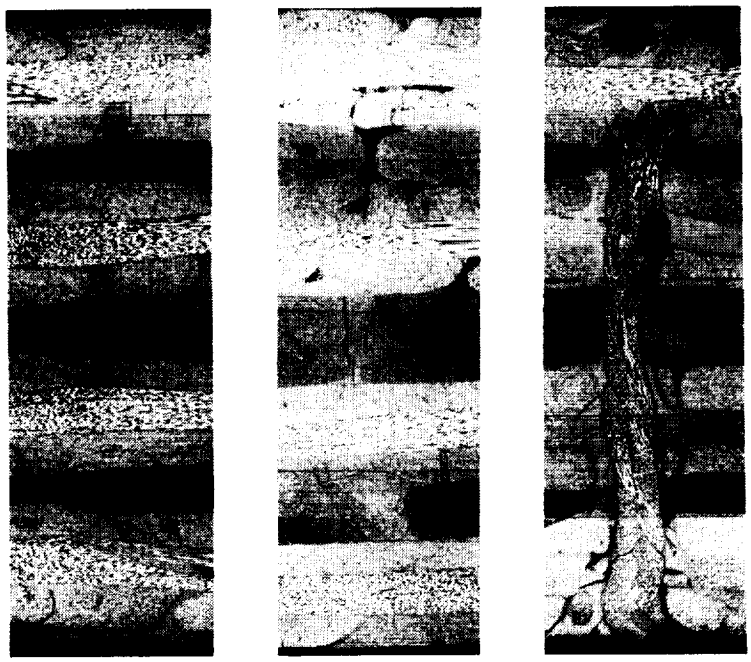

Figure 10 - Photomicrographs through three areas of the stitched panel.

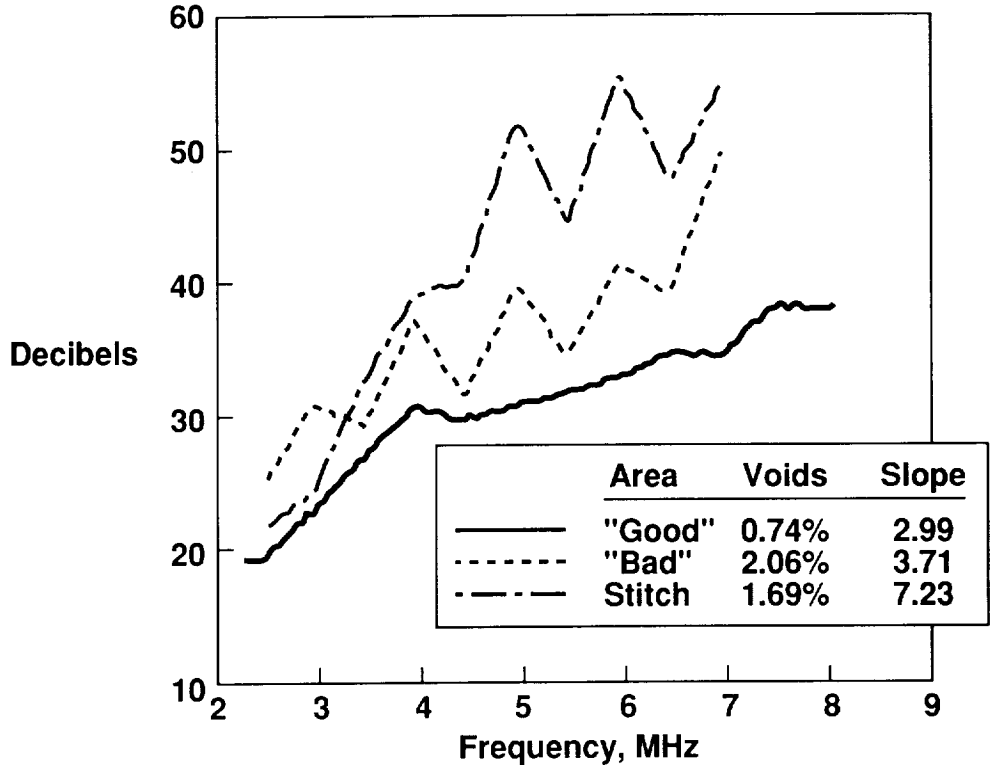

Figure 11 - Differences of Fourier transforms for good, bad, and stitch areas in figure 10. Void content determined from optical analysis.